PNAS RESEARCH ARTICLE | PHYSIOLOGY OPEN ACCESS

Dual amplification strategy turns TRPM2 channels into supersensitive central heat detectors

Ádám Bartók[a,b,c] and László Csanády[a,b,c,1]

Edited by David Clapham, HHMI, Ashburn, VA; received July 19, 2022; accepted October 12, 2022

The Ca^{2+} and ADP ribose (ADPR)-activated cation channel TRPM2 is the closest homolog of the cold sensor TRPM8 but serves as a deep-brain warmth sensor. To unravel the molecular mechanism of heat sensing by the TRPM2 protein, we study here temperature dependence of TRPM2 currents in cell-free membrane patches across ranges of agonist concentrations. We find that channel gating remains strictly agonist-dependent even at 40°C: heating alone or in combination with just Ca^{2+}, just ADPR, Ca^{2+} + cyclic ADPR, or H_2O_2 pretreatment only marginally activates TRPM2. For fully liganded TRPM2, pore opening is intrinsically endothermic, due to ~10-fold larger activation enthalpy for opening (~200 kJ/mol) than for closure (~20 kJ/mol). However, the temperature threshold is too high (>40°C) for unliganded but too low (<15°C) for fully liganded channels. Thus, warmth sensitivity around 37°C is restricted to narrow ranges of agonist concentrations. For ADPR, that range matches, but for Ca^{2+}, it exceeds bulk cytosolic values. The supraphysiological [Ca^{2+}] needed for TRPM2 warmth sensitivity is provided by Ca^{2+} entering through the channel's pore. That positive feedback provides further strong amplification to the TRPM2 temperature response (Q_{10} ~ 1,000), enabling the TRPM2 protein to autonomously respond to tiny temperature fluctuations around 37°C. These functional data together with published structures suggest a molecular mechanism for opposite temperature dependences of two closely related channel proteins.

thermoregulation | transient receptor potential melastatin 2 | thermodynamics | cADPR | kinetics

Temperature sensing in the human body is mediated by members of the transient receptor potential (TRP) ion channel superfamily which consists of several subfamilies (1). Among "thermoTRP" channels, the TRPM subfamily is unique in that it comprises both cold and warm sensors. TRPM8 is the primary detector of environmental cold and also the receptor for cooling agents like menthol or icilin (2). Surprisingly, its closest homolog TRPM2 was recently identified to be warmth-activated and to play a key role in the central regulation of core body temperature (3). Unlike cold-sensing by TRPM8 (4–6), the biophysical background of warmth-sensing by TRPM2 has not yet been studied. Thus, the molecular mechanisms that underlie such opposing modalities of these two closely related channels are unknown.

TRPM family channels share a common tetrameric architecture (7, 8). The transmembrane domain (TMD) and cytosolic N- and C-terminal region of each subunit form a transmembrane pore and a large bell-shaped cytosolic structure which surrounds a central cavity. In homotetrameric TRPM2, a unique C-terminal NUDT9-homology (NUDT9H) domain extends that cytosolic structure with an additional ringlike layer (9, 10). TRPM2 is a Ca^{2+}-permeable nonselective cation channel and is coactivated by cytosolic Ca^{2+} and ADP ribose (ADPR) (11, 12). Each subunit binds one Ca^{2+} ion at the membrane-cytosol interface of the TMD and two molecules of ADPR at two distinct sites: the "N-site" formed by the N-terminal region and the "C-site" formed by the NUDT9H domain (10). In all TRPM2 orthologs, ADPR binding to the N-site drives channel gating. In invertebrate TRPM2 channels, the C-site does not contribute to gating, but in human TRPM2, its role is unclear (10, 13, 14).

Human body temperature is tightly controlled and is kept within a narrow range of ~37±1°C. The preoptic area (POA) of the hypothalamus serves as the central thermostat: warmth-sensitive POA neurons increase their firing rate upon warming, and that signal initiates peripheral autonomous responses that promote heat dissipation. During systemic inflammation, inhibition by prostaglandin E_2 of warmth-sensitive POA neurons causes fever (15). Little is known about the mechanism that drives these POA responses. The central thermostat must contain a temperature sensor that is able to differentiate temperature fluctuations as small as ±1°C around 37°C, but to date, no protein that intrinsically possesses such properties is known. Recently, TRPM2 was identified as the warmth-activated channel pivotal for thermoregulation. Knocking out TRPM2 caused excessive fever

Significance

Thermoregulation in the mammalian body is mediated by a central brain thermostat. Because deep-brain temperatures are maintained within a narrow range, the thermostat must contain a sensor that can differentiate temperature fluctuations as small as ±1°C around 37°C. No protein with such intrinsic properties is currently known. Recently, the ligand-gated ion channel TRPM2 was identified as pivotal for thermoregulation, but it is unclear whether the intrinsic properties of TRPM2 itself or temperature dependence of its agonist concentrations is responsible. Here, we show that the TRPM2 protein intrinsically possesses the unique properties essential for a deep brain temperature sensor: exceptional response-steepness and an optimal threshold. We uncover two unusual molecular mechanisms that serve to achieve that aim in a protein-autonomous manner.

Author contributions: L.C. designed research; Á.B. performed research; L.C. contributed new reagents/analytic tools; Á.B. and L.C. analyzed data; and Á.B. and L.C. wrote the paper.

The authors declare no competing interest.

This article is a PNAS Direct Submission.

[1]To whom correspondence may be addressed. Email: csanady.laszlo@med.semmelweis-univ.hu.

This article contains supporting information online at https://www.pnas.org/lookup/suppl/doi:10.1073/pnas.2212378119/-/DCSupplemental.

Published November 21, 2022.

responses, and pharmacological modulation of TRPM2-positive POA neurons allowed modulation of core body temperature (3, 16). These findings, in line with documented temperature dependence of other TRPM2-dependent processes such as macrophage activation (17) and insulin secretion (18), have outlined TRPM2 as a warmth-activated ion channel.

For all thermoTRP channels, the fractional change in current size over a range of 10°C (Q_{10}) is large (~20–40) compared to other ion channels (~2–4), and the temperature thresholds and response steepnesses have adapted to match their specific physiological roles. To function as the POA heat sensor, TRPM2 would require a temperature threshold of ~37°C and an extremely large Q_{10} value. But whether it indeed possesses such biophysical properties is unknown, as its heat-activation was so far demonstrated only in intact cells, and might therefore reflect either intrinsic heat-sensitivity or temperature-dependent changes in cytosolic agonist concentrations. The multiple proposed mechanisms include TRPM2 activation by heat alone (19), lowering of its temperature threshold by oxidative stress (17), and activation by cyclic ADPR (cADPR) at higher temperatures ((19), cf., (20)).

Here we study temperature dependence of TRPM2 unitary conductance and pore gating in cell-free patches of the membrane, under direct control over cytosolic ligand concentrations and temperature. We find that TRPM2 is intrinsically heat sensitive and identify two mechanisms that turn it into an exquisitely sensitive (Q_{10} ~ 1000) autonomous heat detector in the physiological temperature range (37–40°C). Comparison of these functional data with published cryo-electronmicroscopic (cryo-EM) structures offers insight into how a common TRPM-family structural framework has evolved into both the most steeply cold-activated (TRPM8) and the most steeply warm-activated (TRPM2) thermoTRP channel.

Results

TRPM2 Remains Strictly Ligand-Gated Even at 40°C. Human TRPM2 channels were expressed in HEK-293 cells. Because wild-type (WT) TRPM2 currents irreversibly inactivate within tens of seconds (*SI Appendix*, Fig. S1*A*) (12), for most of this study (Figs. 1–4) we employed the noninactivating T5L pore mutant (*SI Appendix*, Fig. S1*B*) (21) which leaves gating properties intact (*SI Appendix*, Fig. S1 *D–G*) and allows observation of TRPM2 gating at steady state. To ensure perfect control over local cytosolic [Ca^{2+}] even during pronounced TRPM2 activity, Ca^{2+} was omitted from the extracellular (pipette) solution ($[Ca^{2+}]_{free}$ ~ 2 μM). All cytosolic solutions contained 200 μM cytosolic AMP to block endogenous TRPM4-like channels (*SI Appendix*, Fig. S2) and 10 μM dioctanoyl-phosphatydyl-inositol-4,5-bisphosphate (PIP_2) to mimic more closely cellular conditions and to overcome variations in endogenous concentrations of this essential cofactor (21). TRPM2 current (e.g., Fig. 1 *A* and *B*, *Bottom Panels*) and the temperature in the immediate vicinity of the patch (e.g., Fig. 1 *A* and *B*, *Top Panels*) were simultaneously recorded (*Materials and Methods*).

In the complete absence of agonists, raising the temperature from ~25°C (Fig. 1 *A* and *B*, *Top*; gray bars) to ~40°C (Fig. 1 *A* and *B*, *Top*; rose bars) did not elicit TRPM2 channel openings (Fig. 1 *A* and *B*, *Bottom*). In patches containing hundreds of active channels, occasional unitary openings can be resolved at 25°C in the presence of only one agonist (12). To test whether higher temperatures might allow such "semiliganded" channels to open, patches were exposed to saturating (32 μM) ADPR with Ca^{2+} buffered to zero (~4 nM) using ethylene glycol-bis(β-aminoethylether)-N,N,N′,N′-tetraacetic acid (EGTA) (Fig. 1*A*), or to saturating (>100 μM; see *SI Appendix*, Table S1) Ca^{2+} with zero ADPR (Fig. 1*B*), at both 25°C (Fig. 1 *A* and *B*, *Left*) and 40°C (Fig. 1 *A* and *B*, *Right*). Although unitary channel openings were readily resolved at 40°C under such semiliganded conditions (Fig. 1 *A* and *B*, *Insets*), these currents remained negligible when compared to the currents elicited by bracketed exposures to (near-) saturating concentrations of both agonists in the same patches. Thus, even at 40°C, TRPM2 open probability (P_o) remains vanishingly small in the absence of agonists or in the presence of either agonist alone (Fig. 1*C*).

cADPR and H_2O_2 Are Not Direct TRPM2 Activators Even at 40°C. Early reports of TRPM2 activation by high concentrations of cADPR at room temperature (23–25) were later shown to be due to contamination of commercial cADPR preparations with ADPR (22,26). To address reported TRPM2 activation by cADPR at higher temperatures (19, 20), patches were alternately exposed to saturating Ca^{2+} (Fig. 1*D*, black bars) and either 32 μM ADPR or 10 μM cADPR (Fig. 1*D*, gray bars) at both 25°C and 40°C. Although by thin-layer chromatography (TLC), ADPR contamination was not detectable in our "crude" cADPR stock ("cADPR(c)"), exposure to Ca^{2+}+ cADPR(c) evoked measurable currents that were enhanced at 40°C and were significantly larger than those evoked by Ca^{2+} alone (Fig. 1*D*). However, when cADPR was pretreated with the isolated, purified phosphohydrolase domain of *Nematostella vectensis* TRPM2, an enzyme that degrades ADPR but not cADPR (27), exposure to such "purified" cADPR ("cADPR(p)") caused no current enhancement relative to that evoked by Ca^{2+} alone, even at 40°C (Fig. 1*E*; I(cADPR(p) + Ca^{2+})/I(Ca^{2+}) = 1.08 ± 0.11 (n = 5) (P = 0.51)).

Pretreatment of TRPM2-expressing cells with H_2O_2 reportedly sensitizes TRPM2 channels to subsequent heat-induced activation (17). However, in cell-free inside-out patches, a 1-min exposure to an excessive concentration (10 mM) of H_2O_2 followed by heating to 40°C evoked no TRPM2 channel openings, even though in the same patches, exposure to ADPR + Ca^{2+} activated large macroscopic TRPM2 currents (Fig. 1*F*).

Opening of Fully Liganded TRPM2 Is Strongly Endothermic, but the Temperature Threshold Is Far Too Low. We next examined temperature dependence of currents of fully liganded TRPM2 channels in the presence of saturating Ca^{2+}+ADPR. Relative to 25°C, macroscopic steady-state currents were reduced by ~threefold at ~15°C (Fig. 2 *A* and *C*, black) and increased by ~1.5-fold at 37°C (Fig. 2 *B* and *C*, black), revealing intrinsic temperature dependence of currents of fully liganded TRPM2. Similar experiments on patches with smaller numbers of channels (N ≤ 15), in which individual gating transitions could be clearly resolved (Fig. 2 *D* and *E*), allowed dissection of temperature effects on unitary conductance, P_o, and gating kinetics (*Materials and Methods*). Unitary current amplitude (*i*) steadily increased with temperature (Fig. 2 *F* and *G*, black symbols) by ~twofold between 15°C and 37°C. The estimated Q_{10} of 1.36 ± 0.02 (Fig. 2*G*, black fit line) resembles that of the diffusion coefficient of Na^+ ions in water (~1.3), suggesting that at the applied negative membrane potential (−80 mV) Na^+ influx through the TRPM2 pore is near diffusion limited (28). P_o increased from ~0.3 at 15°C to ~0.9 at 25°C, with little further enhancement at higher temperatures (Fig. 2*G*, magenta symbols). The overall effect of temperature on macroscopic

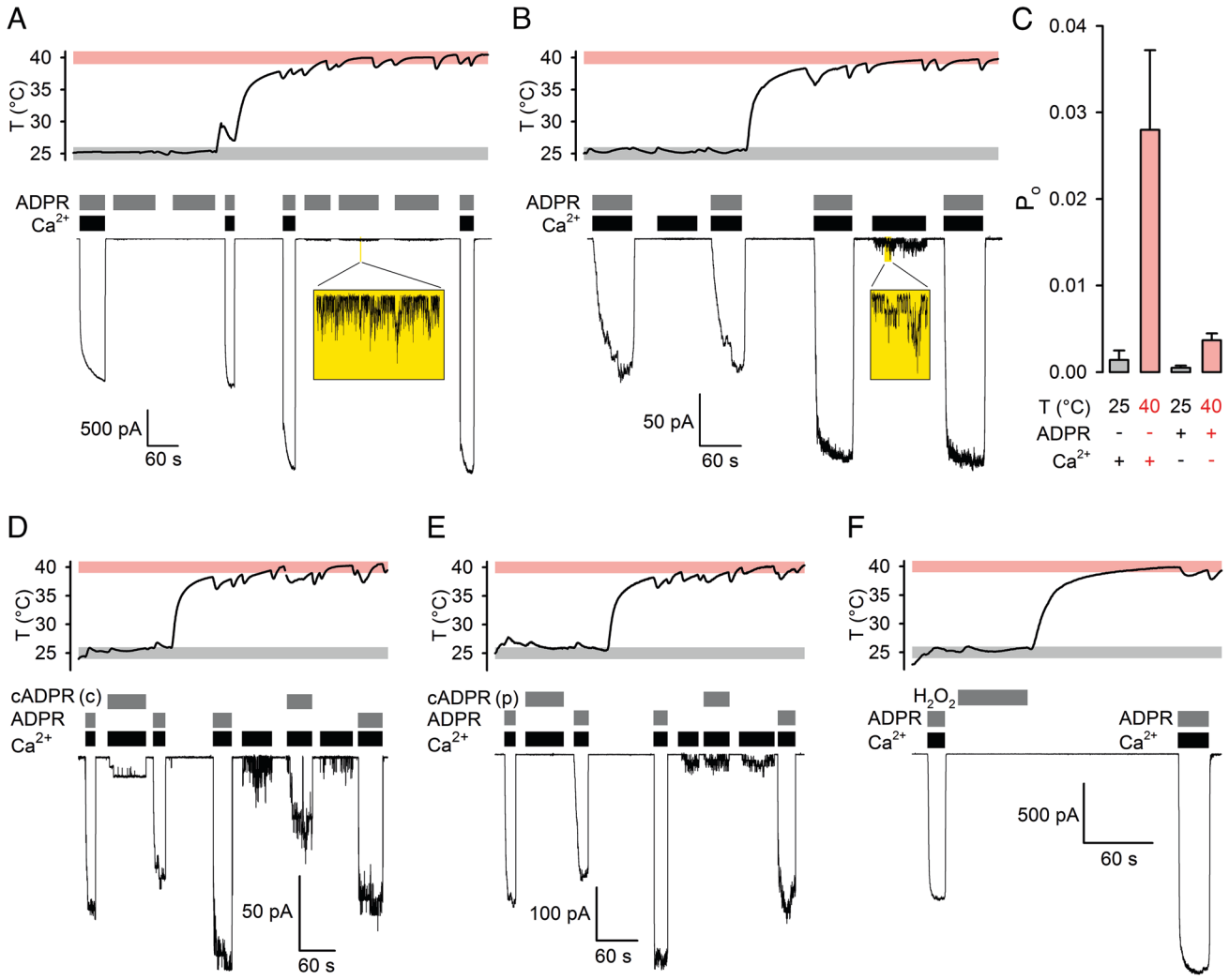

Fig. 1. ADPR+Ca^{2+} is required to efficiently open TRPM2 even at 40°C. *A*, *B*, *D–F*, Simultaneous recordings of patch temperature (*Top Panels*) and macroscopic T5L TRPM2 currents (*Bottom Panels*). In all temperature panels, gray and rose boxes highlight 25±1°C and 40±1°C ranges, respectively; membrane potential (V_m) was −80 mV. *A*, *B*, TRPM2 currents at 25°C and 40°C in (*A*) saturating (32 μM) ADPR + zero Ca^{2+} or (*B*) saturating (107–134 μM) Ca^{2+} + zero ADPR. Resolvable unitary currents (see *Insets*) are quantified by bracketing exposures to saturating (107–134 μM) Ca^{2+} plus saturating (*A*, 32 μM) or quasi-saturating (*B*, 3.2 μM) ADPR. *C*, Estimated P_o under semiliganded conditions at 25°C and 40°C. Bars represent mean ± SEM (n = 6–13). *D*, *E*, TRPM2 currents evoked by cADPR at 25°C and 40°C. Untreated (*D*) "crude" (cADPR(c)) or enzymatically decontaminated (*E*) "pure" (cADPR(p)) cADPR (10 μM) was applied in the presence of saturating (107–134 μM) Ca^{2+}. Currents are quantified by bracketing exposures to saturating (107–134 μM) Ca^{2+} + quasi-saturating (3.2 μM) ADPR at both temperatures. *F*, No TRPM2 current evoked by 1-min treatment with 10 mM H_2O_2 followed by heating, and large currents activated in the same patch by exposures to saturating (32 μM) ADPR + saturating (107–134 μM) Ca^{2+}.

TRPM2 current is fully accounted for by the effects on unitary conductance and gating: the product $i{\cdot}P_o$ normalized to that at 25°C (Fig. 2*C*, purple symbols) closely matches fractional effects of temperature on macroscopic currents (Fig. 2*C*, black symbols).

To better understand the biophysical principles that allow TRPM2 to function as a warmth sensor, we extracted the thermodynamic parameters of gating for fully liganded TRPM2. TRPM2 gating is characterized by long bursts of openings interspersed by brief (2–5 ms) flickery closures and flanked by long (>100 ms) interburst closures, but P_o depends primarily on the slow (interburst↔burst) gating process (12, 29). To dissect activation enthalpies ($\Delta H^{\ddagger}$) and entropies ($\Delta S^{\ddagger}$) of the closed↔open (i.e., interburst↔burst) conformational transition of a fully liganded channel, we performed steady-state gating analysis (*Materials and Methods*) in saturating Ca^{2+}+ADPR at 14°C, 25°C, and 37°C (cf., Fig. 2 *D* and *E*). Temperature-dependence of $P_{o;max}$ (Fig. 2*G*, magenta symbols) is caused by pronounced temperature sensitivity of the long interburst closed time (Fig. 2*H*, blue diamonds), whereas mean burst durations are little affected by temperature (Fig. 2*H*, dark blue circles). Of note, in the maintained presence of 10 μM dioctanoyl-PIP_2, bursts are severalfold longer compared to those observed in the absence of the cofactor (29). From the slopes of Eyring plots (Fig. 2*I*), the activation enthalpy is large for opening ($\Delta H^{\ddagger}_{T-C}$ ~ 200 kJ/mol) but small for closure ($\Delta H^{\ddagger}_{T-O}$ ~ 20 kJ/mol). Accordingly, the van't Hoff plot (Fig. 2*J*) reports an open–closed standard enthalpy difference of ΔH^{0}_{O-C} ~ 183 kJ/mol.

The open–closed standard free enthalpy difference — calculated from the closed–open equilibrium constant $\widehat{P}_{max} = P_{o;max}/(1-P_{o;max})$ — is ΔG^{0}_{O-C} ~ −6 kJ/mol at 25°C, and the absolute gating rates afford an upper estimate of the activation free enthalpy barrier ($\Delta G^{\ddagger}$) at that temperature (Fig. 2*K*; blue profile; smear indicates direction of uncertainty; see *Materials and Methods*). Finally, gating-associated entropy changes are obtained as $\Delta S^{0} = \Delta H^{0} - \Delta G^{0}$ (Fig. 2*K*; green profile; smear indicates direction of

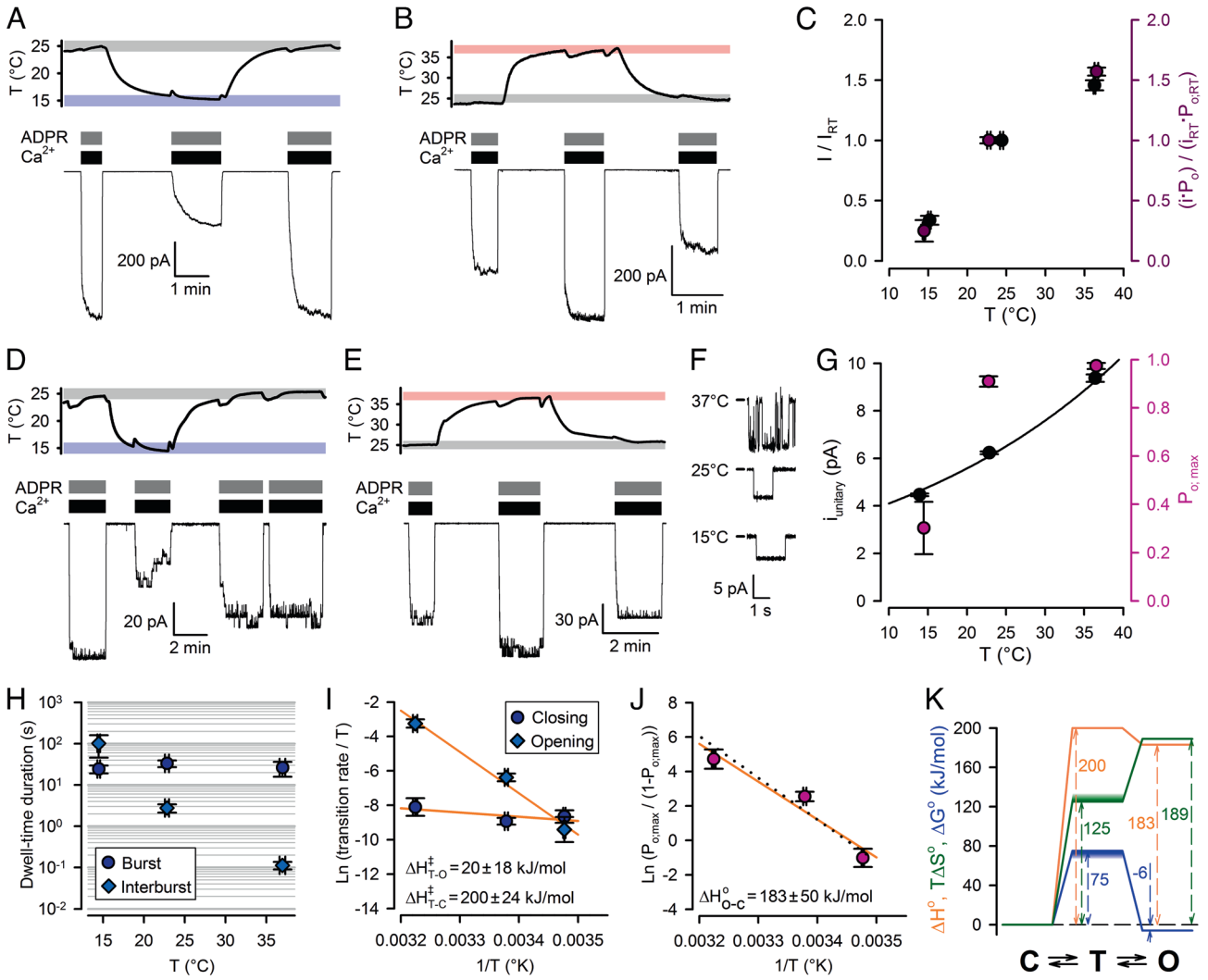

Fig. 2. Temperature dependence of conductance and gating of fully liganded TRPM2. *A*, *B*, *D–E*, Simultaneous recordings of patch temperature (*Top Panels*) and T5L TRPM2 currents (*Bottom Panels*). In temperature panels, gray, rose, and blue boxes highlight 25±1°C, 37±1°C, and 15±1°C ranges, respectively; V_m was −80 mV. Large macroscopic currents (*A*, *B*) or smaller currents with resolvable unitary gating events (*D*, *E*) in response to exposures to saturating ADPR + saturating Ca^{2+} at 25°C and 15°C (*A*, *D*) or 25°C and 37°C (*B*, *E*). [Ca^{2+}] was 477, 134, and 113 μM, respectively, at 15°C, 25°C, and 37°C, and [ADPR] was 32 μM. *C*, (Black symbols) Steady-state macroscopic currents at the three temperatures, normalized to the mean of the currents in bracketing segments at 25°C within the same patch. (Purple symbols) Product of unitary current (*i*) and P_o at the three temperatures, normalized to the average value of $i \cdot P_o$ at 25°C. *F*, T5LTRPM2 unitary currents at 15°C, 25°C, and 37°C. *G*, P_o (magenta symbols) and *i* (black symbols) at the three temperatures. Black line is a least-squares fit of *i* by the function $i(T) = i(22) \cdot Q_{10}^{(T-25)/10}$ (T: temperature in °C). Data in *C*, *G* represent mean ± SEM, n = 8–18 (*C*, black), 5–6 (*C*, purple), 3–10 (*G*, black), 6–17 (*G*, magenta). *H*, Mean burst (dark blue circles) and interburst (blue diamonds) durations of fully liganded TRPM2 as a function of temperature. *I*, Eyring plots of closing (dark blue circles) and opening (blue diamonds) rate of fully liganded TRPM2 constructed from the data in panel *H*; orange lines are linear regression fits yielding the plotted activation enthalpies. *J*, van't Hoff plot of fully liganded TRPM2 constructed from the data in panel *G* (magenta); orange line is a linear regression fit yielding the plotted standard enthalpy of opening. Black dotted line, prediction of the Fig. 4*A* model fit to the data in Fig. 4 *B* and *C*. Data in *H–J* represent mean ± SEM, n = 5–15. *K*, thermodynamic profile of slow gating of fully liganded TRPM2 (C: closed (interburst) state; T: transition state; O: open (bursting) state). Standard enthalpies (orange), free enthalpies (blue), and entropies (green) are plotted relative to the closed (interburst) state as a reference. Uncertainties in transition-state free enthalpy and entropy are represented by smears.

uncertainty in $\Delta S^{\ddagger}$). The obtained thermodynamic profiles (Fig. 2*K*) reveal that opening of a fully liganded TRPM2 channel is associated with a large positive enthalpy change compensated by a large increase in entropy. These biophysical characteristics are the exact opposite of those of TRPM8 (4, 5).

Manipulation of Agonist Concentrations Provides Room for Temperature Threshold Adjustment. Although the closed–open equilibrium constant of fully liganded TRPM2 proved to be strongly temperature dependent (Fig. 2*J*; $Q_{10} > 10$), its temperature threshold is far too low (<15°C) to be physiologically relevant: at ~37°C, $P_{o;max}$ approaches unity and thus depends only modestly on temperature. However, temperature sensitivity might be enhanced at subsaturating agonist concentrations. Because channel activator ligands bind more tightly to the open channel, apparent affinities ($K_{1/2}$) of agonists depend on the maximal open probability: ligand dose–response curves are shifted leftward or rightward, respectively, by conditions that increase or decrease $P_{o;max}$. To test the impact of a temperature-dependent $P_{o;max}$ on agonist $K_{1/2}$ values, TRPM2 current activation by test concentrations of Ca^{2+} in the presence of saturating ADPR (Fig. 3 *A* and *C*), or by test concentrations of ADPR in the presence of saturating Ca^{2+} (Fig. 3 *B* and *D*), were recorded at 14°C (Fig. 3 *A* and *B*) and 40°C (Fig. 3 *C* and *D*) and compared to the currents observed at the respective temperatures during bracketing exposures to saturating concentrations of both ligands. The obtained dose–response curves of fractional current activation (Fig. 3 *E* and *F*) indeed revealed strong temperature dependence of apparent agonist affinities:

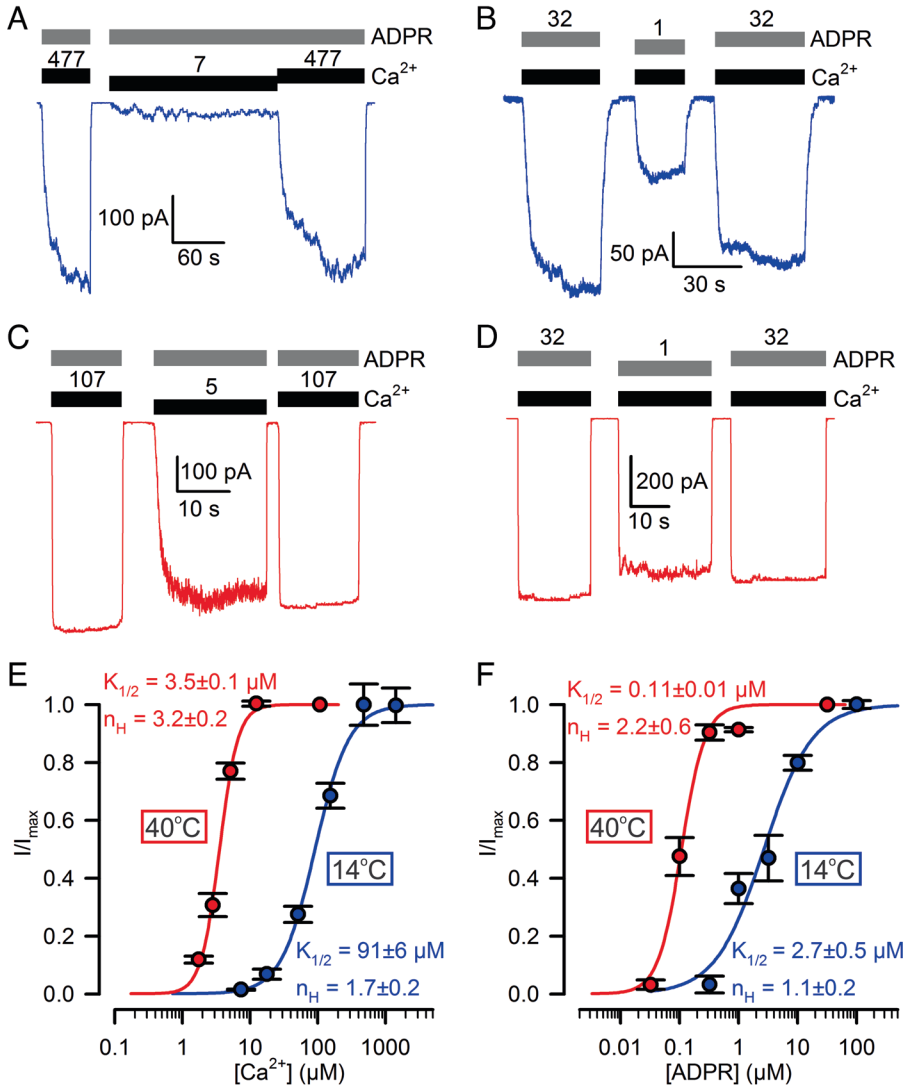

Fig. 3. Apparent affinities of TRPM2 for both ADPR and Ca^{2+} are strongly temperature dependent. *A–D*, Macroscopic T5L TRPM2 currents at (*A*, *B*) 14°C and (*C*, *D*) 40°C, evoked by (*A*, *C*) 32 μM ADPR (gray bars) and various concentrations of Ca^{2+} (black bars, [Ca^{2+}] in μM), or (*B*, *D*) saturating Ca^{2+} (black bars) and various concentrations of ADPR (gray bars, [ADPR] in μM). [Ca^{2+}] was 477 and 107 μM, respectively, at 14°C and 40°C; V_m was −80 mV. *E*, *F*, Dose–response curves at 14°C (blue symbols) and 40°C (red symbols) of macroscopic T5L TRPM2 currents for (*E*) Ca^{2+} and (*F*) ADPR, with the other ligand kept saturated. Currents were normalized to the mean of the currents observed during bracketing exposures to saturating Ca^{2+} + ADPR in the same patch. Data in *E*, *F* represent mean ± SEM, n = 4–20 (*E*, blue), 6–9 (*E*, red), 3–10 (*F*, blue), 4–12 (*F*, red). Colored curves are fits to the Hill equation with fit parameters plotted in the panels.

$K_{1/2}$ for Ca^{2+} (in saturating ADPR) decreased from ~90 μM to ~3 μM (Fig. 3*E*, blue and red fit line) and $K_{1/2}$ for ADPR (in saturating Ca^{2+}) from ~3 μM to ~0.1 μM (Fig. 3*F*, blue and red fit line), between 14°C and 40°C. These results suggest that in living cells, adjustment of agonist concentrations might be exploited to shift the threshold for TRPM2 temperature activation into a physiologically relevant range.

Monod–Wyman–Changeux Mechanism Adequately Describes TRPM2 Gating Across a Broad Range of [ADPR], [Ca^{2+}], and Temperatures. To quantitatively assess the relationship between agonist concentrations and temperature sensitivity, we obtained experimental P_o estimates across broad concentration ranges of both ligands at temperatures spanning 14–40°C (Fig. 4 *B* and *C*, colored symbols). P_o values were estimated by rescaling the normalized macroscopic agonist dose–response curves obtained at 25°C (*SI Appendix*, Fig. S1 *E–G*), 14°C, and 40°C (Fig. 3 *E* and *F*) with the measured absolute P_o values of fully liganded channels at those three temperatures (Fig. 2*G*, magenta; for 40°C $P_{o;max}$~1). We then attempted to describe this entire data set using a mechanistic gating model.

TRPM2 agonist binding stoichiometries can be described by a two-dimensional scheme, with zero to four molecules of bound Ca^{2+} and ADPR (for simplicity, we consider only ADPR bound at the N-site to be strongly relevant for gating). Thus, states C_{ij} and O_{ij} represent the closed and open conformations, respectively, of a channel with *i* molecules of Ca^{2+} and *j* molecules of ADPR bound (Fig. 4*A*; open states for lower ligand stoichiometries have been omitted for clarity); the same pair of subscripts identifies the gating equilibrium constant ($\widehat{P}_{ij}$) and the standard thermodynamic parameters (i.e., ΔH^0_{ij}, ΔG^0_{ij}, ΔS^0_{ij}) of the $C_{ij} \leftrightarrow O_{ij}$ transition. TRPM2 gating by Ca^{2+} in saturating ADPR (Fig. 4*A*, green shading) is well described (12) by the Monod–Wyman–Changeux mechanism which postulates that agonist binding to the four subunits is independent but affects concerted gating transitions in an energetically equivalent, additive manner (30). Extending that mechanism also

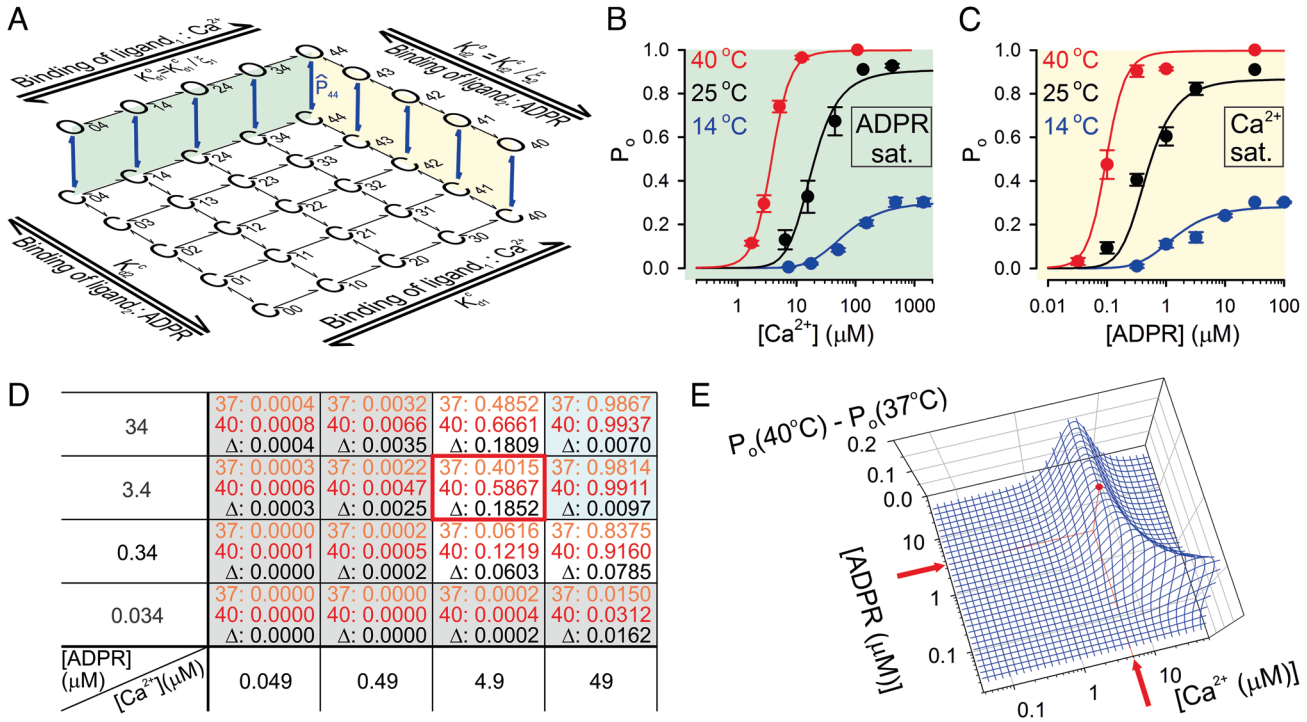

[ADPR] (μM) \ [Ca2+] (μM)	0.049	0.49	4.9	49
34	37: 0.0004 40: 0.0008 Δ: 0.0004	37: 0.0032 40: 0.0066 Δ: 0.0035	37: 0.4852 40: 0.6661 Δ: 0.1809	37: 0.9867 40: 0.9937 Δ: 0.0070
3.4	37: 0.0003 40: 0.0006 Δ: 0.0003	37: 0.0022 40: 0.0047 Δ: 0.0025	37: 0.4015 40: 0.5867 Δ: 0.1852	37: 0.9814 40: 0.9911 Δ: 0.0097
0.34	37: 0.0000 40: 0.0001 Δ: 0.0000	37: 0.0002 40: 0.0005 Δ: 0.0002	37: 0.0616 40: 0.1219 Δ: 0.0603	37: 0.8375 40: 0.9160 Δ: 0.0785
0.034	37: 0.0000 40: 0.0000 Δ: 0.0000	37: 0.0000 40: 0.0000 Δ: 0.0000	37: 0.0002 40: 0.0004 Δ: 0.0002	37: 0.0150 40: 0.0312 Δ: 0.0162

Fig. 4. Temperature threshold of TRPM2 is optimized for physiological [ADPR] but supraphysiological [Ca^{2+}]. *A*, Simplified model of TRPM2 gating by Ca^{2+} and ADPR; open states O_{00}... O_{33} are omitted for clarity. Green and yellow shadings highlight the subschemes that describe gating in saturating ADPR and saturating Ca^{2+}, respectively. $\hat{P}_{44}$, closed–open equilibrium constant of fully liganded TRPM2; ξ_1 and ξ_2, coupling constants of the two agonists; K^C_{d1} and K^O_{d1}, dissociation constants of Ca^{2+} from closed and open channels, respectively; K^C_{d2} and K^O_{d2}, dissociation constants of ADPR from closed and open channels, respectively. (By the principle of detailed balance $K^O_{d1} = K^C_{d1} / \xi_1$ and $K^O_{d2} = K^C_{d2} / \xi_2$). *B*, *C*, TRPM2 open probability in (*B*) various [Ca^{2+}] plus saturating ADPR and (*C*) various ADPR plus saturating [Ca^{2+}] at 14°C (red symbols), 25°C (black symbols), and 40°C (blue symbols). Colored curves represent ensemble fit of the scheme in panel *A* to the entire data set using four free parameters (see text for details); the fitted values are ΔH^0_{44} = +202 kJ/mol, ΔS^0_{44} = +696 $Jmol^{-1}K^{-1}$, K^C_{d1} = 16.6 μM, and K^C_{d2} = 0.35 μM. *D*, P_o values calculated from the fitted model for a range of [Ca^{2+}] and [ADPR] at 37°C (orange numbers) and 40°C (red numbers), and $\Delta P_o = P_o(40°C) - P_o(37°C)$ (black numbers). The red frame marks the maximum point for ΔP_o, and shaded cells identify agonist concentration ranges in which P_o is ~0 (gray) or ~1 (cyan) at both temperatures. *E*, Three-dimensional mesh plot of ΔP_o as a function of [Ca^{2+}] and [ADPR]; the red dot identifies the maximum point.

to gating by ADPR ("ligand 2") (Fig. 4*A*; yellow shading), P_o as a function of [Ca^{2+}] and [ADPR] is described by the equation

$$P_o = \frac{\hat{P}_{44}}{\hat{P}_{44} + \left(\frac{K^C_{d1} + [Ca^{2+}]}{K^C_{d1}/\xi_1 + [Ca^{2+}]}\right)^4 \left(\frac{K^C_{d2} + [ADPR]}{K^C_{d2}/\xi_2 + [ADPR]}\right)^4}. \quad [1]$$

Here, $\hat{P}_{44}$ is the gating equilibrium constant of fully liganded channels (transition $C_{44} \leftrightarrow O_{44}$). K^C_{d1} and K^C_{d2} are the dissociation constants of Ca^{2+} and ADPR, respectively, from closed channels, whereas ξ_1 and ξ_2 are the "coupling constants" (31) that describe their efficacies to promote channel opening (i.e., the factor by which binding of each agonist molecule increases the gating equilibrium constant: $\xi_1 = \hat{P}_{i+1;j} / \hat{P}_{i;j}$ and $\xi_2 = \hat{P}_{i;j+1} / \hat{P}_{i;j}$).

Although in principle each of the five parameters in Eq. **1** might be temperature dependent, as a first approximation, we tested to what extent temperature dependence of $\hat{P}_{44}$ alone might account for the data. Magnitude and temperature dependence of $\hat{P}_{44}$ is defined by ΔH^0_{44} and ΔS^0_{44} (the standard enthalpy and entropy of the $C_{44} \leftrightarrow O_{44}$ transition) through the equation

$$\hat{P}_{44} = e^{-\frac{\Delta H^0_{44}}{RT}} \cdot e^{\frac{\Delta S^0_{44}}{R}}. \quad [2]$$

To further reduce the number of free parameters, both coupling constants were tentatively fixed to ~30, based on an earlier estimate of ξ_1 (12). Intriguingly, an ensemble fit of our set of six dose–response curves (Fig. 4 *B* and *C*, colored symbols) by this constrained model with only four free parameters (ΔH^0_{44}, ΔS^0_{44}, K^C_{d1}, and K^C_{d2}) provided a reasonable description of TRPM2 open probability across a broad range of agonist concentrations and temperatures (Fig. 4 *B* and *C*, colored lines; fit parameters in legend).

Temperature Threshold of TRPM2 Is Optimized for Physiological [ADPR] but Supraphysiological [Ca^{2+}]. The temperature threshold of fully liganded TRPM2 is <15°C (Fig. 2*G*). To perform its physiological function as a sensor of core body temperature, a threshold of ~37°C is required. The model in Fig. 4*A*, with its fitted parameters, allows to calculate the agonist concentration ranges in which that condition is met. Using the model, we calculated the extent of channel activation between 37°C and 40°C, i.e., $\Delta P_o = P_o(40°C) - P_o(37°C)$ for a range of [Ca^{2+}] and [ADPR] (Fig. 4*D*). At low concentrations of both agonists (Fig. 4*D*, gray cells), P_o ~ 0 both at 37°C (Fig. 4*D*, orange numbers) and at 40°C (Fig. 4*D*, red numbers), whereas at high concentrations of both agonists (Fig. 4*D*, cyan cells), P_o ~ 1 at both temperatures—thus, ΔP_o (Fig. 4*D*, black numbers) is ~0 under both conditions. Consequently, substantially large values of ΔP_o are limited to a narrow range of intermediate agonist concentrations, reaching a maximum value of ΔP_o ~ 0.19 at [Ca^{2+}] = 4.9 μM, [ADPR] = 3.4 μM (Fig. 4*D*, red frame). A continuous plot of ΔP_o as a function of [Ca^{2+}] and [ADPR] (Fig. 4*E*, blue mesh) reveals that ΔP_o remains near maximal around that peak (Fig. 4*E*, red dot) when the concentrations of the two agonists are varied in opposite directions. It also shows that, even when the other agonist is abundant, substantial ΔP_o is not achieved below [Ca^{2+}] ~ 2 μM or [ADPR] ~ 0.1 μM. For ADPR, that threshold falls well within

the physiological range (22), but the Ca^{2+}-threshold is above the physiological range of bulk cytosolic [Ca^{2+}] which typically remains <1 μM.

Positive Feedback by Ca^{2+} Influx Through the Pore Endows TRPM2 with Extreme Temperature Sensitivity. In the TRPM2 structure, the binding sites for activating Ca^{2+} are within 3 nm of the cytosolic pore entrance and are directly connected to it by four tunnels (9, 10, 32). Because the TRPM2 pore is Ca^{2+} permeable, the local [Ca^{2+}] around the cytoplasmic channel surface is largely influenced by Ca^{2+} entering through the pore (12, 33, 34) and is expected to be higher than bulk cytosolic [Ca^{2+}] (cartooned in Fig. 5*F*). We therefore investigated how the presence of a physiological concentration of extracellular Ca^{2+} affects temperature dependence of TRPM2 gating between 37°C and 40°C. Because the T5L mutation increases Ca^{2+} permeability (21), for these experiments, WT TRPM2 channels were employed. Indeed, in the presence of ~1 mM extracellular (pipette) Ca^{2+}, macroscopic WT TRPM2 currents were readily activated at both temperatures by cytosolic superfusion with physiological concentrations of 2 μM ADPR + 0.1 μM (bulk) Ca^{2+} (Fig. 5 *A* and *B*), confirming that local [Ca^{2+}] around the activating sites must have risen well above 1 μM under such conditions (cf., Fig. 4*D*). As observed at 25°C (*SI Appendix*, Fig. S1*A*), WT TRPM2 currents inactivated within tens of seconds also at these physiological temperatures (Fig. 5 *A* and *B*). Rundown of WT TRPM2 reflects an irreversible progressive decline in the number of active channels, while the P_o of the surviving active channel pool remains relatively constant (12). To estimate that P_o under the above conditions at 37°C and 40°C, the same protocol was applied but interrupted by a brief exposure to saturating cytosolic agonist concentrations that allowed sampling of the current amplitude under fully liganded conditions,

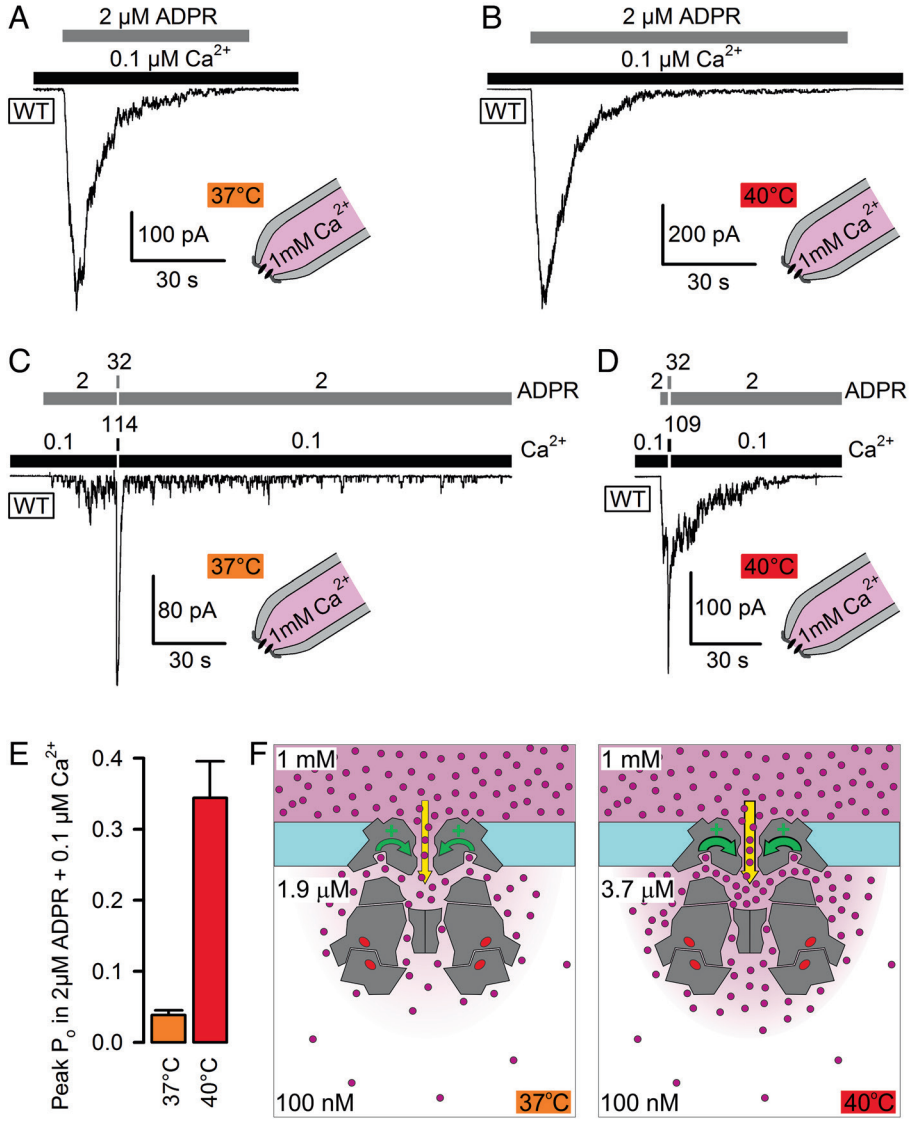

Fig. 5. Positive feedback by Ca^{2+} influx enhances TRPM2 temperature sensitivity. *A–D*, Transient activation of macroscopic inside-out patch currents of WT TRPM2 channels at 37°C (*A*, *C*) and 40°C (*B*, *D*) by cytosolic superfusion with 0.1 μM Ca^{2+} + 2 μM ADPR, with ~1 mM free Ca^{2+} present in the extracellular (pipette) solution. In *C*, *D*, cytosolic agonist concentrations were briefly (for ~1.5 s) raised to saturating levels (concentrations indicated above bars; in μM). V_m was −80 mV. *E*, Estimated P_o (mean ± SEM, n = 11) of transiently active WT TRPM2 channels at 37°C and 40°C in the presence of cytosolic 0.1 μM (bulk) Ca^{2+} + 2 μM ADPR and ~1 mM extracellular Ca^{2+}. *F*, Cartoon representation of WT TRPM2 activity at 37°C (*Left*) and 40°C (*Right*). Cross sections through TRPM2 structure (gray) outline the pore, the cytosolic cavity, the activating Ca^{2+} binding sites, and tunnels connecting these sites to pore and cytosol. Magenta dots, Ca^{2+} ions; red ovals, ADPR bound to N- and C-sites. Magenta shading scales with local [Ca^{2+}]. At 40°C, higher local [Ca^{2+}] around the activating sites (black numbers) provides stronger positive feedback (curved green arrows) to pore gating.

i.e., when P_o ~ 1. Based on the gating kinetics of ligand-saturated channels (Fig. 2*H*) at 37°C (τ_b ~ 30 s; τ_{ib} ~ 0.1 s), the expected time constant of current activation in response to such sudden agonist "spiking" ($\tau_{relax} = 1/((1/\tau_b) + (1/\tau_{ib}))$) is ~0.1 s at 37°C and <0.1 s at 40°C, consistent with the time constants observed for the dominant (>90%) fractions of macroscopic currents activated by longer ligand exposures at those two temperatures (Figs. 1, 2 *B* and *E*, and 3 *C* and *D*; see also *SI Appendix*, Fig. S3 *A* and *B*). Thus, a 1–2 s exposure to saturating ligand concentrations was chosen to allow for near-complete current relaxation while minimizing rundown during the test spike. Fractional current enhancement by the resulting transient current spikes (Fig. 5 *C* and *D*) was >20-fold at 37°C (Fig. 5*C*) but only ~threefold at 40°C (Fig. 5*D*), reporting P_o values of ~0.04 and ~0.34, respectively, at 37°C and 40°C in the presence of physiological agonist concentrations (Fig. 5*E*, difference significant at $P < 0.01$). Of note, fractional stimulation was not correlated with the time lag between the onset of channel activation and subsequent agonist spiking (*SI Appendix*, Fig. S3 *A–C*), confirming that the P_o of the surviving channel population is indeed relatively constant throughout the entire process of macroscopic current rundown (see also gating pattern of last open channels in *SI Appendix*, Fig. S3 *A* and *B*). Because such a large ΔP_o cannot be achieved at any fixed concentration of agonists (Fig. 4*E*), these findings directly demonstrate and also quantitate the positive feedback provided by Ca^{2+} influx. The larger P_o at 40°C elevates local [Ca^{2+}] around the activating sites, which in turn further enhances P_o. From the measured P_o values and [ADPR] = 2 μM, the calculated (Eq. **1**) steady-state local [Ca^{2+}] is ~1.9 μM at 37°C but ~3.7 μM at 40°C (Fig. 5*F*), despite continuous vectorial rinsing of the cytosolic patch surface with a solution buffered to 100 nM Ca^{2+} using 144 mM gluconate + 1 mM EGTA. Thus, Ca^{2+} influx through the pore not only ensures that local [Ca^{2+}] rises above the threshold required for heat sensitivity at body temperature (Fig. 4*E*), but the positive feedback also provides tremendous amplification to the temperature responsiveness, yielding an ~eightfold increase in P_o across a temperature range of just 3°C, equivalent to a Q_{10} of ~1,000. Consistent with that interpretation, the activating effect of extracellular Ca^{2+} could be largely blunted by excessive cytosolic Ca^{2+} buffering using 10 mM of the fast Ca^{2+} buffer 1,2-bis(o-aminophenoxy)ethane-N,N,N′,N′-tetraaceticacid (BAPTA) (*SI Appendix*, Fig. S4).

Discussion

The results presented here provide insight into two aspects of TRPM2 structure-function: the biophysical mechanisms that allowed a common TRPM structural framework to evolve into both cold- and heat-activated channels and the molecular strategy that has made TRPM2 suitable to function as an exquisitely sensitive deep-brain temperature sensor under physiological conditions.

Heating Alone Is Insufficient for, and H_2O_2 or cADPR Are Not Involved in, TRPM2 Activation. In the past, various explanations for the activation of TRPM2 whole-cell currents by high temperatures have been suggested. The present experiments in cell-free membrane patches refute several of these hypotheses. We show here that heating alone, in the absence of agonists, is insufficient to activate TRPM2 (Fig. 1), suggesting that activation of TRPM2 whole-cell currents by heating (19) must rely on the endogenous presence of its agonists in cells. Moreover, we show here that the simultaneous presence of both Ca^{2+} and ADPR is required for efficient TRPM2 activation even at temperatures as high as 40°C (Fig. 1 *A–C*). These findings contrast with a study which reported activation of TRPM2 whole-cell currents by Ca^{2+} alone in HEK-293 cells (35). Although we also observed Ca^{2+}-evoked unitary TRPM2 channel openings (Fig. 1 *B*, *Inset*), quantitation of P_o reveals that activity to be small, even at 40°C (Fig. 1 *C*, *Left*). The reason for that difference is unclear, but we note that in our patches excised from untransfected control HEK-293 cells, cytosolic application of Ca^{2+} often activated variable-size currents from endogenous cation channels with biophysical properties similar to those of TRPM4, which could be blocked by cytosolic AMP without affecting TRPM2 currents (*SI Appendix*, Fig. S2). Given that TRPM4 is reportedly expressed in HEK-293 cells (36), care must be taken to avoid contamination of whole-cell TRPM2 currents in HEK-293 cells by potentially present endogenous TRPM4-like currents that may activate secondary to TRPM2-mediated Ca^{2+} influx.

TRPM2 was originally identified as a channel activated by oxidative stress (37, 38), but later studies concluded that such activation is indirect, mediated by oxidative stress-induced accumulation of cytosolic ADPR (26, 39). More recently, pretreatment with H_2O_2 of HEK-293 cells expressing mouse TRPM2 was shown to lower the threshold for subsequent heating-induced activation of TRPM2 whole-cell currents (17). Because that sensitization could be averted by TRPM2 mutation M214A, it was interpreted to reflect direct H_2O_2-induced oxidation of methionine 214. However, in the cryo-EM structure of hsTRPM2, the equivalent residue (M215) contacts ADPR bound at the N-site, and mutation M215A robustly reduces ADPR-induced TRPM2 current, suggesting that it interferes with ADPR binding (10). We show here that exposure of cell-free patches to an excessive concentration (10 mM) of H_2O_2 fails to confer heating-induced activation to TRPM2 (Fig. 1*F*). Thus, temperature-sensitivity of TRPM2 currents is not enhanced by direct oxidation of the TRPM2 protein.

Early studies conducted at room temperature identified cADPR as a low-affinity ($K_{1/2}$ ~ 50–700 μM) TRPM2 activator (23–25), but that agonistic effect was later shown to be eliminated by enzymatic removal of contaminant ADPR from cADPR stocks (22,26). Interestingly, in recent cryo-EM structures of human TRPM2, the N-site accommodates ADPR in a horseshoe-like bent conformation which resembles that of cADPR (10), prompting the proposal that direct cADPR binding to the N-site activates TRPM2 at higher temperatures (19, 20). Here, we show that cADPR devoid of contaminating ADPR is not a TRPM2 agonist even at 40°C (Fig. 1*E*), consistent with a recent report (40). Considering the extremely high sensitivity of TRPM2 for ADPR at 40°C ($K_{1/2}$ ~ 0.1 μM; Fig. 3*F*), as little as ~1% of contaminating ADPR — well below the detection limit by TLC — is sufficient to account for substantial TRPM2 activation by 10 μM untreated cADPR at 40°C (Fig. 1*D*). Thus, cADPR binding is not involved in TRPM2 activation in response to heating.

Molecular Mechanism of Temperature Sensing in TRPM2. A large activation enthalpy for opening but small activation enthalpy for closure (Fig. 2*I*) underlies the large positive standard enthalpy of TRPM2 pore opening (Fig. 2 *J* and *K*). Intriguingly, that thermodynamic profile is the exact opposite of that of its closest relative TRPM8 (4, 5). Moreover, unlike TRPM2 which is strictly ligand-dependent (Fig. 1), TRPM8 can be opened by low temperature alone (41). Such pronounced functional dichotomy suggests, despite a common TRPM structural framework, fundamentally different gating-associated conformational changes in the two channels. Indeed, a comparison of cryo-EM structures of multiple TRPM8 and TRPM2 orthologs in several conformations reveals profoundly different molecular motions. For TRPM8, alignments of the closed (apo) structure (42, 43) with

an agonist-bound preopen structure (44), or with a Ca^{2+}-bound open-desensitized structure (43), reveal substantial conformational rearrangements that are largely confined to the TMD region and the TRP helix, whereas the majority of the cytosolic region, which encompasses ~80% of the protein's volume, remains relatively static (Movie S1). Moreover, in TRPM8, both activators (cooling agents) and inhibitors bind to the TMDs. In contrast, for TRPM2 comparison of the Ca^{2+}+ADPR-bound fully open (zebrafish) or preopen (human) structures with the respective closed (apo) structures reveals a dramatic rearrangement of the large cytosolic region associated with pore opening (9, 10): the ring formed by the MHR1/2 regions (central layer) expands whereas those formed by the MHR3/4 regions (top layer) and the NUDT9H domains (bottom layer) contract (Movie S1). Overall these rearrangements, promoted by ADPR binding to the N-site, are accompanied by the disruption of multiple intra- and inter-subunit interfaces and an increase in disorder, explaining the large positive standard enthalpy and entropy of opening (Fig. 2*K*, orange and green profiles). Based on the thermodynamic profile of the activation barrier, most bonds are already broken in the transition state (Fig. 2*K*, state T), but this is followed by further substantial increase in disorder as the channel relaxes to the open state (Fig. 2*K*, state O).

Because opening-associated movements of the TMD region and the TRP-helix are similar for TRPM8 and TRPM2 (9, 43), we speculate that the perhaps intrinsically exothermic (or thermoneutral) nature of opening-associated TMD/TRP-helix motions of a TRPM-family channel is overpowered in TRPM2 by the coupled strongly endothermic process of cytosolic domain rearrangements. That mechanism might be shared by TRPM4 and TRPM5 channels which are also heat activated (45). Indeed, in closed TRPM4 (46), inhibitory nucleotides bind at the same intersubunit interface (the "resting interface") that is disrupted in TRPM2 upon opening (10), suggesting that nucleotides inhibit TRPM4 by stabilizing that intersubunit contact. However, experimental validation of that hypothesis will be challenging. First, from a functional point of view, it will require determination of the true enthalpy of gating of unliganded TRPM2, and dissection of the extent to which the enthalpies of binding of the two agonists Ca^{2+} and ADPR, as well as the differences in binding enthalpy to a closed vs. an open channel, contribute to the overall thermodynamic profile of a fully liganded TRPM2 channel. In that regard, our present data set did not provide sufficient constraints to fit Eq. **1** while leaving temperature dependence for all five of its parameters free. Moreover, although our kinetic model (Fig. 4*A*) includes binding of only one ADPR molecule per subunit (at the N-site), it remains to be established whether ADPR binding to the C-site might also contribute to gating in human TRPM2 (cf., 47). Second, from a structural point of view, it will require determination of the extent of cytosolic domain movements associated with pore opening of unliganded channels. Finally, it is even less clear whether the molecular mechanisms underlying similarly positive temperature dependences are shared between TRPM2 and its more distant relatives TRPV1/TRPV2 (48), which lack the entire large TRPM-specific cytosolic region. Interestingly, allosteric coupling of endothermic domain movements to pore opening is a mechanism that has been suggested also for TRPV1 (49).

Physiological Implications for Central Thermoregulation. We show here that in TRPM2, ligand binding is exploited to shift the temperature activation threshold into a physiologically relevant range. Because unliganded TRPM2 does not open at physiological temperatures (Fig. 1) whereas fully liganded channels are near-maximally active (Fig. 2*G*, magenta), significant temperature responsiveness of TRPM2 around 37°C requires submaximal agonist binding stoichiometries and is therefore restricted to a narrow range of Ca^{2+} and ADPR concentrations (Fig. 4 *D* and *E*). For ADPR, that range spans the submicromolar-to-low micromolar regime and therefore matches the range of cellular [ADPR] estimates (0.1–5 μM; (22,50)). Interestingly, for Ca^{2+}, the required concentration (>2 μM) exceeds the range of bulk cytosolic [Ca^{2+}] observed in neurons even during a high-frequency stimulus train (51) and is found only in localized microdomains within nanometers of an active Ca^{2+} source (52). We show here that at body temperature, sporadic TRPM2 openings occur in the presence of ADPR even in the virtual absence (~4 nM) of Ca^{2+} (Fig. 1 *A*, *Inset* and *C*, *Right*). Because the TRPM2 pore is Ca^{2+} permeable (11, 53) and the binding sites for activating Ca^{2+} are very near the cytosolic pore entrance (10, 12), in the presence of ADPR and physiological extracellular Ca^{2+}, each TRPM2 channel is able to generate its own Ca^{2+} nanodomain required for activity. That mechanism might ensure relative independence of TRPM2 temperature sensing from other Ca^{2+}-dependent cellular signaling pathways. Indeed, we show here that under physiological conditions, local [Ca^{2+}] around the activating sites of a WT TRPM2 channel rises into the micromolar range and supports robust channel currents (Fig. 5 *A*, *B*, and *F*). Moreover, the positive feedback on channel gating by local Ca^{2+} lends unexpected steepness to the TRPM2 temperature response, yielding an ~eightfold increase in P_o over a range of 3°C (Fig. 5*E*). The extrapolated value of Q_{10} ~ 1,000 is the highest ever reported for an ion channel. That estimate obviously depends on the extent of cytosolic Ca^{2+} buffering, as it can be largely reduced by excessive concentrations of a fast Ca^{2+} buffer (10 mM BAPTA, *SI Appendix*, Fig. S4). However, our experimental conditions, i.e., vectorial rinsing of the cytosolic channel surface by a continuously flowing low-Ca^{2+} bath solution buffered with 144 mM gluconate + 1 mM EGTA (Fig. 5), represent relatively strong buffering compared to the static cytosol of most live neurons (54). Thus, under in vivo conditions, the extent of positive feedback might be even stronger and explains how TRPM2 is able to serve as an efficient detector of the extremely limited fluctuations in deep brain temperature (15).

Materials and Methods

Expression of Human TRPM2 Channels in HEK 293 Cells. Control HEK 293T cells were obtained from ATCC (CRL-11268). HEK 293 cells stably expressing WT TRPM2 were purchased from SB Drug Discovery. HEK 293T cells transiently expressing T5L TRPM2 and green fluorescent protein (GFP) were generated by cotransfecting HEK 293T cells with T5L-TRPM2/pcDNA3 and GFP/pcDNA3 at a 10:1 ratio (FuGENE HD transfection reagent, Promega). HEK 293 cells stably expressing T5L TRPM2 were kindly provided by Katalin Zboray (Agricultural Institute, Centre for Agricultural Research, Martonvásár, Hungary). All cells were cultured at 37°C in 5% CO_2 in Dulbecco'sModified Eagle's Medium (DMEM) medium with 4.5 g/L glucose (Lonza) supplemented with 10% Fetal Bovine Serum (FBS) (EuroClone), 2 mM L-glutamine, and 100 units/ml penicillin/streptomycin (Lonza).

Enzymatic Purification of cADPR. To remove contaminating ADPR from commercial cADPR, 0.2 μM purified nvNUDT9-H protein (27) was added to the bath solution containing 10 μM cADPR and incubated for >10 min at room temperature before recording.

Inside-Out Patch Recordings. WT TRPM2 currents were recorded in inside-out patches from HEK 293 cells stably expressing WT TRPM2. T5L TRPM2 currents were recorded in inside-out patches from HEK 293 cells stably or transiently expressing T5L TRPM2. Endogenous cation channel currents were studied in inside-out patches from untransfected HEK 293T cells. Pipette (extracellular) solution contained (in mM) 140 Na-gluconate, 2 Mg-$gluconate_2$, and 10 piperazine-N,N′-bis(2-ethanesulfonicacid) (PIPES) (pH 7.4 with NaOH at 25°C). A 140 mM NaCl-based solution for the pipette electrode was carefully layered on top (12). For the recordings in Fig. 5 *A*–*D*, 8 mM Ca-$gluconate_2$ was added

to the pipette solution to obtain ~1 mM free [Ca^{2+}]. Bath (cytosolic) solution contained (in mM) 140 Na-gluconate, 2 Mg-gluconate$_2$, and 10 4-(2-hydroxyethyl)-1-piperazineethanesulfonicacid (HEPES) (pH 7.1 with NaOH). Free [Ca^{2+}] was adjusted by adding (i) 0–10 mM Ca-gluconate$_2$ (to obtain ~1.7–1,400 μM free [Ca^{2+}]; *SI Appendix*, Table S1), (ii) 1 mM EGTA (to obtain "zero" (~4 nM) free [Ca^{2+}]), or (iii) 1 mM EGTA and 240 μM Ca-gluconate$_2$ (to obtain ~100 nM free Ca^{2+}); free [Ca^{2+}] was spectrophotometrically determined at each temperature (*SI Appendix, SI Materials and Methods* and Fig. S5). All bath solutions also contained 200 μM AMP and 10 μM dioctanoyl-PIP_2. The bath electrode (in 3 M KCl) was connected to the cytosolic solution through a KCl-agar bridge. For the recordings at different target temperatures, pH of the bath solutions was adjusted to 7.1 at the given temperature. Temperature-dependent changes in pH of the pipette solution were kept minimal by the use of PIPES buffer ($\Delta pK_a/10°C = -0.085$). Following excision, patches were transferred to a flow chamber in which the continuously flowing bath solution could be exchanged (time constant <100 ms) using electronic valves (ALA-VM8, ALA Scientific Instruments). During recordings, the temperatures of the flow lines were controlled using Peltier-driven temperature controllers (TC-10 Dagan Corporation), and the patch temperature was monitored using a BAT-12 microprobe thermometer (Physitemp) positioned in the bath flow at a distance of ~2 mm from the membrane patch. TRPM2 channel activating ligands – Ca^{2+} (Ca-gluconate$_2$; Sigma-Aldrich), ADPR (Sigma-Aldrich), and dioctanoyl-PIP_2 (Cayman Chemical) – and all other nucleotides (AMP, ADP, MgATP (Sigma-Aldrich), and cADPR (Biolog Life Science Institute)) were dissolved into the bath solution from >100x concentrated, pH-adjusted aqueous stocks. Currents were recorded at a bandwidth of 2 kHz (Axopatch 200B; Molecular Devices), digitized at 10 kHz (Digidata 1322A; Molecular Devices), and saved to disk (Pclamp10; Molecular Devices).

Analysis of Macroscopic Current Recordings. Macroscopic fractional currents (Figs. 2*C*, black and 3 *E–F* and *SI Appendix*, Figs. S1 *E, G* and S2*B*) were calculated as the mean of the steady current under a test condition (i.e., test concentration of an agonist, or test temperature) normalized to the mean of the steady-state currents in bracketing segments of record under reference conditions (i.e., in the presence of maximal agonist concentrations or at the reference temperature (25°C)) recorded from the same patch. Dose–response curves were fitted to the Hill equation using least squares.

Estimation of Unitary Current Amplitudes. Unitary current amplitudes (Fig. 2*G*, black and *SI Appendix*, Figs. S1*C* and S2*C*) were estimated from current amplitude histograms as the distances between adjacent peaks of fits by sums of Gaussian functions.

Kinetic Analysis of Microscopic Current Recordings. To estimate gating kinetics in the presence of saturating agonist concentrations, segments of record with 1–15 active channels with well-resolved unitary gating transitions were Gaussian filtered at 50 Hz and idealized by half-amplitude threshold crossing. P_o (Fig. 2*G*, magenta) was determined from the resulting events lists as $(\sum_k I_k \cdot t_k)/(N \cdot T)$, where I_k and t_k denote the conductance level and duration of the k^{th} event, N is the number of active channels in the patch, and T is the total duration of the analyzed segment. Even for the T5L construct, a slow rundown (progressive decline in N) was observed in some recordings (e.g., Figs. 1 *D* and *E* and 2 *B* and *D*), requiring individual estimation of N in each segment of record analyzed. In high-P_o (P_o ~ 0.9 or higher) segments, obtained at temperatures of 25–40°C, N was estimated as the maximum number of simultaneously open channels. In low-P_o test segments at 14°C, N was linearly interpolated between those of the bracketing reference segments. P_o dose–response curves at 14°C, 25°C, and 40°C (Fig. 4 *B* and *C*) were constructed by rescaling the macroscopic dose–response curves (Fig. 3 *E* and *F* and *SI Appendix*, Figs. S1 *E* and *G*) with the P_o of fully liganded channels at the respective temperatures (Fig. 2*G*, magenta symbols; P_o assumed ~1 at 40°C).

Slow gating parameters were obtained by fitting the C_1–O_3–C_2 scheme (where C_1 and C_2 represent the long and brief closed states, respectively) to the sets of dwell-time histograms using maximum likelihood, while correcting for an imposed fixed dead time of 6 ms (55). Mean burst (τ_b) and interburst (τ_{ib}) durations (Fig. 2*H*) were calculated from the fitted rate constants as $\tau_b = (1/k_{31})(1 + (k_{32}/k_{23}))$, $\tau_{ib} = 1/k_{13}$. For a more detailed description of the algorithm and its application to TRPM2, see refs. 29 and 55.

Estimation of Thermodynamic Parameters. To obtain ΔH^0_{O-C} (Fig. 2*J*), the equilibrium constant of the closed–open transition was calculated at each temperature as $\widehat{P} = P_o/(1 - P_o)$, and ΔH^0_{O-C} was obtained as $-R$ times the slope of an ln $\widehat{P}$ vs. $1/T$ plot (van't Hoff plot; T is temperature in °K; $R = 8.13$ Jmol^{-1}K^{-1}). To obtain activation enthalpies for the slow opening ($\Delta H^{\ddagger}_{T-C}$) and slow closing ($\Delta H^{\ddagger}_{T-O}$) transition (Fig. 2*I*), opening and closing rates were defined as $k_{CO}=1/\tau_{ib}$ and $k_{OC}=1/\tau_b$, and $\Delta H^{\ddagger}$ values were obtained as $-R$ times the slope of ln(k/T) vs. $1/T$ plots (Eyring plots).

Thermodynamic profiles of slow gating (Fig. 2*K*) were constructed as described (56). The standard enthalpy profile was constructed from ΔH^0_{O-C} and $\Delta H^{\ddagger}_{T-C}$. To construct the standard free enthalpy (ΔG^0) profile, ΔG^0 between open and closed ground states was calculated as $\Delta G^0_{O-C} = -RT$ ln $\widehat{P}$. Free enthalpy barriers were estimated using Eyring theory (57). Upper estimates of activation free enthalpies ($\Delta G^{\ddagger}_{max}$) at 25°C were obtained from the absolute values of the opening and closing rates using the Eyring equation with a transmission coefficient (κ) of 1. E.g., $\Delta G^{\ddagger}_{T-C;max} = RT\ln(k_B T/(k_{CO}h))$, where k_B is Boltzmann's constant ($k_B = 1.38 \cdot 10^{-23}$ J/°K) and h is Planck's constant ($h = 6.63 \cdot 10^{-34}$ Js). Because κ might be smaller than 1, the true value of $\Delta G^{\ddagger}$ might be lower (see smear in Fig. 2*K*, blue profile). The standard entropy profile was obtained as $T\Delta S^0 = \Delta H^0 - \Delta G^0$.

Model Fitting. To fit the model in Fig. 4*A* to the data, the ensemble of the six dose–response curves in Fig. 4 *B* and *C* was fitted by Eq. **1**; the sum of the squared errors was minimized using a simplex algorithm (58). Out of the five parameters in Eq. **1** ($\widehat{P}_{44}$, K^C_{d1}, K^C_{d2}, ξ_1, and ξ_2), only $\widehat{P}_{44}$ was assumed to be temperature dependent, expressed as a function of ΔH^0_{44} and ΔS^0_{44} (Eq. **2**), and the constraint $\xi_1 = \xi_2 = 30$ was applied. Allowing for temperature dependence of K^C_{d1}, K^C_{d2}, ξ_1, and ξ_2 did not substantially improve the fit. Thus, the data did not provide sufficient constraint to reliably estimate the temperature dependences of the latter four parameters.

Statistics. All data are shown as mean ± SEM with the number of independent experiments (n) indicated in each panel. Differences were considered significant for $P < 0.05$, using Student's t test.

Data, Materials, and Software Availability. All data are included in the article and/or *SI Appendix*.

ACKNOWLEDGMENTS. We thank Beáta Töröcsik for subcloning T5L-TRPM2 into pcDNA3, Iordan Iordanov for providing purified nvNUDT9H, and Katalin Zboray (Agricultural Institute, Centre for Agricultural Research, Martonvásár, Hungary) for providing the stable T5L TRPM2 cell line (Economic Development and Innovation Operational Programme (GINOP-2.3.2-15-2016-00051) of the National Research, Development and Innovation Office). Support was provided by EU Horizon 2020 Research and Innovation Program grant 739593 and MTA Lendület grant LP2017-14/2017 to L.C. and a New National Excellence Program (ÚNKP) award of the Ministry of Human Capacities of Hungary to Semmelweis University. Á.B. was supported by the János Bolyai Research Scholarship of the Hungarian Academy of Sciences (BO/00103/20) and the New National Excellence Program (ÚNKP) Bolyai+ scholarship of the Ministry of Human Capacities of Hungary (ÚNKP-20-5-SE-6 and ÚNKP-21-5-SE-10).

Author affiliations: [a]Hungarian Centre of Excellence for Molecular Medicine-Semmelweis Egyetem (HCEMM-SE) Molecular Channelopathies Research Group, Semmelweis University, Budapest H-1094, Hungary; [b]Magyar Tudományos Akadémia-Semmelweis Egyetem (MTA-SE) Ion Channel Research Group, Semmelweis University, Budapest H-1094, Hungary; and [c]Department of Biochemistry, Semmelweis University, Budapest H-1094, Hungary

1. X. Steinberg, C. Lespay-Rebolledo, S. Brauchi, A structural view of ligand-dependent activation in thermoTRP channels. *Front. Physiol.* **5**, 171 (2014).
2. D. D. McKemy, W. M. Neuhausser, D. Julius, Identification of a cold receptor reveals a general role for TRP channels in thermosensation. *Nature* **416**, 52–58 (2002).
3. K. Song *et al.*, The TRPM2 channel is a hypothalamic heat sensor that limits fever and can drive hypothermia. *Science.* **353**, 1393–1398 (2016).
4. T. Voets *et al.*, The principle of temperature-dependent gating in cold- and heat-sensitive TRP channels. *Nature* **430**, 748–754 (2004).

5. S. Brauchi, P. Orio, R. Latorre, Clues to understanding cold sensation: Thermodynamics and electrophysiological analysis of the cold receptor TRPM8. *Proc. Natl. Acad. Sci. U.S.A.* **101**, 15494–15499 (2004).
6. I. Díaz-Franulic *et al.*, A folding reaction at the C-terminal domain drives temperature sensing in TRPM8 channels. *Proc. Natl. Acad. Sci. U.S.A.* **117**, 20298–20304 (2020).
7. Y. Huang *et al.*, A structural overview of the ion channels of the TRPM family. *Cell Calcium* **85**, 102111. (2020).
8. A. Szollosi, Two decades of evolution of our understanding of the transient receptor potential melastatin 2 (TRPM2) cation channel. *Life (Basel)* **11**, (2021).
9. Y. Huang *et al.*, Architecture of the TRPM2 channel and its activation mechanism by ADP-ribose and calcium. *Nature* **562**, 145–149 (2018).
10. Y. Huang, B. Roth, W. Lu, J. Du, Ligand recognition and gating mechanism through three ligand-binding sites of human TRPM2 channel. *Elife.* **8**, pii: e50175 (2019).
11. A. L. Perraud *et al.*, ADP-ribose gating of the calcium-permeable LTRPC2 channel revealed by Nudix motif homology. *Nature* **411**, 595–599 (2001).
12. L. Csanády, B. Torocsik, Four Ca2+ ions activate TRPM2 channels by binding in deep crevices near the pore but intracellularly of the gate. *J. Gen. Physiol.* **133**, 189–203 (2009).
13. F. J. Kuhn *et al.*, ADP-ribose activates the TRPM2 channel from the sea anemone Nematostella vectensis independently of the NUDT9H domain. *PLoS One* **11**, e0158060. (2016).
14. B. Tóth, I. Iordanov, L. Csanády, Selective profiling of N- and C-terminal nucleotide-binding sites in a TRPM2 channel. *J. Gen. Physiol.* **152**, (2020).
15. J. Siemens, G. B. Kamm, Cellular populations and thermosensing mechanisms of the hypothalamic thermoregulatory center. *Pflugers Arch.* **470**, 809–822 (2018).
16. G. B. Kamm *et al.*, A synaptic temperature sensor for body cooling. *Neuron* **109**, 3283–3297 (2021).
17. M. Kashio *et al.*, Redox signal-mediated sensitization of transient receptor potential melastatin 2 (TRPM2) to temperature affects macrophage functions. *Proc. Natl. Acad. Sci. U.S.A.* **109**, 6745–6750 (2012).
18. M. Kashio, M. Tominaga, Redox signal-mediated enhancement of the temperature sensitivity of transient receptor potential melastatin 2 (TRPM2) elevates glucose-induced insulin secretion from pancreatic islets. *J. Biol. Chem.* **290**, 12435–12442 (2015).
19. K. Togashi *et al.*, TRPM2 activation by cyclic ADP-ribose at body temperature is involved in insulin secretion. *EMBO J.* **25**, 1804–1815 (2006).
20. P. Yu *et al.*, Direct gating of the TRPM2 channel by cADPR via specific interactions with the ADPR binding pocket. *Cell Rep.* **27**, 3684–3695 (2019).
21. B. Tóth, L. Csanády, Pore collapse underlies irreversible inactivation of TRPM2 cation channel currents. *Proc. Natl. Acad. Sci. U.S.A.* **109**, 13440–13445 (2012).
22. I. Heiner *et al.*, Endogenous ADP-ribose enables calcium-regulated cation currents through TRPM2 channels in neutrophil granulocytes. *Biochem. J.* **398**, 225–232 (2006).
23. M. Kolisek, A. Beck, A. Fleig, R. Penner, Cyclic ADP-ribose and hydrogen peroxide synergize with ADP-ribose in the activation of TRPM2 channels. *Mol. Cell* **18**, 61–69 (2005).
24. A. Beck *et al.*, Nicotinic acid adenine dinucleotide phosphate and cyclic ADP-ribose regulate TRPM2 channels in T lymphocytes. *FASEB J.* **20**, E47–E54 (2006).
25. I. Lange, R. Penner, A. Fleig, A. Beck, Synergistic regulation of endogenous TRPM2 channels by adenine dinucleotides in primary human neutrophils. *Cell Calcium* **44**, 604–615 (2008).
26. B. Tóth, L. Csanády, Identification of direct and indirect effectors of the transient receptor potential melastatin 2 (TRPM2) cation channel. *J. Biol. Chem.* **285**, 30091–30102 (2010).
27. I. Iordanov, B. Tóth, A. Szollosi, L. Csanády, Enzyme activity and selectivity filter stability of ancient TRPM2 channels were simultaneously lost in early vertebrates. *Elife.* **8**, pii: e44556 (2019).
28. B. Hille, *Ionic Channels of Excitable Membranes* (Sinauer Associates Inc., Sunderland, Massachussetts, 1992).
29. B. Tóth, I. Iordanov, L. Csanády, Putative chanzyme activity of TRPM2 cation channel is unrelated to pore gating. *Proc. Natl. Acad. Sci. U.S.A.* **111**, 16949–16954 (2014).
30. J. Monod, J. Wyman, J. P. Changeux, On the nature of allosteric transitions: A plausible model. *J. Mol. Biol.* **12**, 88–118 (1965).
31. A. Auerbach, Thinking in cycles: MWC is a good model for acetylcholine receptor-channels. *J. Physiol.* **590**, 93–98 (2012).
32. Z. Zhang *et al.*, Structure of a TRPM2 channel in complex with Ca(2+) explains unique gating regulation. *Elife.* **7**, pii: e36409 (2018).
33. D. McHugh *et al.*, Critical intracellular Ca2+ dependence of transient receptor potential melastatin 2 (TRPM2) cation channel activation. *J. Biol. Chem.* **278**, 11002–11006 (2003).
34. J. Starkus, A. Beck, A. Fleig, R. Penner, Regulation of TRPM2 by extra- and intracellular calcium. *J. Gen. Physiol.* **130**, 427–440 (2007).
35. J. Du, J. Xie, L. Yue, Intracellular calcium activates TRPM2 and its alternative spliced isoforms. *Proc. Natl. Acad. Sci. U.S.A.* **106**, 7239–7244 (2009).
36. P. Launay *et al.*, TRPM4 is a Ca2+-activated nonselective cation channel mediating cell membrane depolarization. *Cell* **109**, 397–407 (2002).
37. Y. Hara *et al.*, LTRPC2 Ca2+-permeable channel activated by changes in redox status confers susceptibility to cell death. *Mol. Cell* **9**, 163–173 (2002).
38. E. Wehage *et al.*, Activation of the cation channel long transient receptor potential channel 2 (LTRPC2) by hydrogen peroxide. A splice variant reveals a mode of activation independent of ADP-ribose. *J. Biol. Chem.* **277**, 23150–23156 (2002).
39. A. L. Perraud *et al.*, Accumulation of free ADP-ribose from mitochondria mediates oxidative stress-induced gating of TRPM2 cation channels. *J. Biol. Chem.* **280**, 6138–6148 (2005).
40. W. M. Riekehr *et al.*, cADPR Does Not Activate TRPM2. *Int. J. Mol. Sci.* **23** (2022).
41. N. Raddatz *et al.*, Temperature and voltage coupling to channel opening in transient receptor potential melastatin 8 (TRPM8). *J. Biol. Chem.* **289**, 35438–35454 (2014).
42. Y. Yin *et al.*, Structure of the cold- and menthol-sensing ion channel TRPM8. *Science* **359**, 237–241 (2018).
43. M. M. Diver, Y. Cheng, D. Julius, Structural insights into TRPM8 inhibition and desensitization. *Science* **365**, 1434–1440 (2019).
44. Y. Yin *et al.*, Visualizing structural transitions of ligand-dependent gating of the TRPM2 channel. *Nat. Commun.* **10**, 3740 (2019).
45. K. Talavera *et al.*, Heat activation of TRPM5 underlies thermal sensitivity of sweet taste. *Nature* **438**, 1022–1025 (2005).
46. J. Guo *et al.*, Structures of the calcium-activated, non-selective cation channel TRPM4. *Nature* **552**, 205–209 (2017).
47. E. Gattkowski *et al.*, Novel CaM-binding motif in its NudT9H domain contributes to temperature sensitivity of TRPM2. *Biochim. Biophys. Acta Mol. Cell Res.* **1866**, 1162–1170 (2019).
48. J. Yao, B. Liu, F. Qin, Kinetic and energetic analysis of thermally activated TRPV1 channels. *Biophys. J.* **99**, 1743–1753 (2010).
49. A. Jara-Oseguera, C. Bae, K. J. Swartz, An external sodium ion binding site controls allosteric gating in TRPV1 channels. *Elife.* **5**, pii: e13356 (2016).
50. L. Tong, S. Lee, J. M. Denu, Hydrolase regulates NAD+ metabolites and modulates cellular redox. *J. Biol. Chem.* **284**, 11256–11266 (2009).
51. N. Hosoi, T. Sakaba, E. Neher, Quantitative analysis of calcium-dependent vesicle recruitment and its functional role at the calyx of Held synapse. *J. Neurosci.* **27**, 14286–14298 (2007).
52. M. Naraghi, E. Neher, Linearized buffered Ca2+ diffusion in microdomains and its implications for calculation of [Ca2+] at the mouth of a calcium channel. *J. Neurosci.* **17**, 6961–6973 (1997).
53. Y. Sano *et al.*, Immunocyte Ca2+ influx system mediated by LTRPC2. *Science* **293**, 1327–1330 (2001).
54. B. Schwaller, Cytosolic Ca2+ buffers. *Cold Spring Harb. Perspect. Biol.* **2**, a004051. (2010).
55. L. Csanády, Rapid kinetic analysis of multichannel records by a simultaneous fit to all dwell-time histograms. *Biophys. J.* **78**, 785–799 (2000).
56. L. Csanády, A. C. Nairn, D. C. Gadsby, Thermodynamics of CFTR channel gating: A spreading conformational change initiates an irreversible gating cycle. *J. Gen. Physiol.* **128**, 523–533 (2006).
57. I. H. Segel, *Enzyme Kinetics: Behavior and Analysis of Rapid Equilibrium and Steady-State Enzyme Systems* (Wiley, 1993).
58. W. H. Press, W. T. Vetterling, S. A. Teukolsky, B. P. Flannery, *Numerical Recipes in C. The Art of Scientific Computing* (Cambridge University Press, 1992).